Study of turbulent premixed flame propagation using a laminar flamelet model

By H. G. Im

1. Motivation and objectives

The laminar flamelet concept in turbulent reacting flows is considered applicable to many practical combustion systems (Liñán & Williams 1993). For turbulent premixed combustion, the laminar flamelet regime is valid when turbulent Karlovitz number is less than unity, which is equivalent to stating that the characteristic thickness of the flame is less than that of a Kolmogorov eddy; this is known as the Klimov-Williams criterion (Williams 1985). In such a case, the flame maintains its laminar structure, and the effect of turbulent flow is merely to wrinkle and strain the flame front. The propagating wrinkled premixed flame can then be described as an infinitesimally thin surface dividing the unburnt fresh mixture and the burnt product.

It has been suggested (Kerstein *et al.* 1988) that such a propagating front can be represented as a level contour of a continuous function G, whose governing equation, derived using the Huygens' principle, is

$$\rho \frac{\partial G}{\partial t} + \rho u_j \frac{\partial G}{\partial x_j} = \rho s_L |\nabla G|. \tag{1}$$

Here s_L is the well-defined laminar flame speed which is generally not a constant, but can be modified by the effect of flame stretch. By introducing the Markstein length $\mathcal{L}$ (Pelce & Clavin 1982), an asymptotic analysis gives an expression for s_L:

$$s_L = s_L^\circ - s_L^\circ \mathcal{L} \nabla \cdot \mathbf{n} + \mathcal{L} \mathbf{n} \cdot (\nabla \mathbf{n}) \cdot \mathbf{n}, \tag{2}$$

where $\mathbf{n} = -\nabla G / |\nabla G|$ is the normal vector to the surface pointing toward the unburnt mixture. The Markstein length is of the order of flame thickness $\lambda / \rho c_p s_L$ defined usually in terms of unburnt mixture properties. Here λ is the thermal conductivity and c_p the specific heat.

There are several advantages to using the G-equation model rather than direct numerical simulation with Arrhenius-type chemistry. First, since the flame front is described by a contour of the smooth function G, complex topology changes in the propagating front can be easily captured by solving the transport equation for G, instead of tracking the corrugated front. Secondly, since the numerical stiffness due to the Arrhenius chemistry with large activation energy is removed in favor of a flamelet whose structure is given *a priori*, the computational effort can be significantly reduced with an appropriate discontinuity-capturing numerical scheme. Furthermore, the diffusional-thermal modification of the flame structure is accounted for by the flame-speed relation (2) in a parametric manner; the coupling

between the hydrodynamic field and the flame-structure is simply accounted for by the parameter $\mathcal{L}$. This is important in validating the existing predictions of turbulent flame speed, most of which are based on the constant s_L assumption. Finally, by eliminating the nonlinear reaction terms from the conservation equations, the system can be more easily adapted to large-eddy simulation based on the dynamic subgrid-scale modeling principle. A preliminary attempt at such modeling will be discussed in a later section.

From a fundamental standpoint, the G-equation model serves as a useful tool for understanding some issues in turbulent premixed combustion. One such issue is the determination of turbulent flame speed, s_T, as a function of flow quantities such as the turbulence intensity, u'. Although there are theoretical models and experimental observations, the agreement among the various results is far from being satisfactory. Thus far, perhaps the only concensus is that s_T increases with u' initially, then tends to level off at larger u', which is often called "bending" behavior (Bradley 1992).

Most theoretical models of s_T in the flamelet regime are based on Damköhler's (1940) proposition that the increase in the flame speed is proportional to the area increase, which in turn can be related to the turbulence intensity. This suggests

$$s_T/s_L = A_T/A_L \sim 1 + C(u'/s_L)^q, \tag{3}$$

where A_T is the total surface area of the wrinkled front and A_L the cross-section area normal to the direction of propagation. Based on this proposition, Clavin & Williams (1979) derived $q = 2$ from geometrical considerations, while Yakhot's renormalization group theory (1988a) yields the same result in the weak turbulence limit. Recently, Kerstein & Ashurst (1992) proposed $q = 4/3$ by considering the random nature of turbulent flows. This result was further supported by their numerical study (Kerstein & Ashurst 1994).

All of these arguments are based on the constant density assumption so the effect of heat release generated by chemical reaction has not been taken into account. Variable density introduces additional complexities, one being that the coupling between flow and flame must be dealt with. Recently, Cambray & Joulin (1992), in a semi-analytic study of the model equation by Michelson & Sivashinsky (1977), demonstrated that, at least if $u' \leq O(s_L)$, the turbulent burning velocity is noticeably enhanced by hydrodynamic instability. Their numerical results suggest the value q of about 0.3 in the weak turbulence range. If validated by further studies, this result may show that the "bending" behavior may be the effect of thermal-expansion induced wrinkling, which diminishes at higher u'.

Therefore, in this study we attempt to provide a useful database for understanding these issues in turbulent premixed combustion. In particular, the effect of thermal expansion is investigated by fully coupling the G-equation with the flow field. In the following section, the formulation of the variable-density version of the G-equation model is presented, and some numerical results are discussed for premixed flames propagating in a harmonic inlet velocity flow field and a pair of counter-rotating vortices. The results of the former problem are consistent with those of Cambray & Joulin (1992), while the study of the flame-vortex interaction also reveals interesting

behaviors regarding the vorticity produced by flame. Finally, a subgrid-scale model for the G-equation based on the dynamic modeling concept is proposed.

2. Accomplishments

2.1 *The G-equation model with heat release*

2.1.1 *Formulation*

Throughout this study, we define the flame front as the contour, $G = 0$, of a continuous function $G(\mathbf{x}, t)$, where $G < (>)\ 0$ is defined as the unburnt (burnt) side. The species equation is then substituted by the G-equation which can be written in conservative form as (Williams 1985)

$$\frac{\partial}{\partial t}(\rho G) + \frac{\partial}{\partial x_j}(\rho u_j G) = \rho s_L |\nabla G|. \tag{4}$$

Using the flame-speed relation (2) with the definition $\mathbf{n} = -\nabla G / |\nabla G|$, we obtain (Peters 1992)

$$\frac{\partial}{\partial t}(\rho G) + \frac{\partial}{\partial x_j}(\rho u_j G) = \rho_0 s_L^{\circ}\left(|\nabla G| + \mathcal{L}\nabla^2 G - \mathcal{L}\frac{\partial \ln|\nabla G|}{\partial x_j}\frac{\partial G}{\partial x_j}\right)$$

$$+ \rho\mathcal{L}\frac{1}{|\nabla G|}\frac{\partial u_k}{\partial x_j}\frac{\partial G}{\partial x_j}\frac{\partial G}{\partial x_k} \tag{5}$$

where the subscript 0 denotes the condition at the unburnt mixture, s_L° the plane laminar flame speed, and we use the approximation $\rho s_L = \rho_0 s_L^{\circ} = $ constant. Equation (5) accounts for the effect of the flame stretch given by the results (2).

To include the effect of thermal expansion, we introduce the *total energy*

$$e = \frac{1}{2}u_i^2 + c_v T + q[1 - \mathcal{H}(G)] \tag{6}$$

where $\mathcal{H}$ is the Heaviside function. This implies that as the flow crosses the flame $(G = 0)$, an amount of chemical energy q is converted to thermal energy, thereby creating jumps in the density and temperature. The conservation equation for the total energy is free of reaction term, *i.e.*

$$\frac{\partial}{\partial t}(\rho e) + \frac{\partial}{\partial x_j}[(\rho e + P)u_j] = \frac{\partial}{\partial x_j}(u_i \tau_{ij}) - \frac{\partial}{\partial x_i}\left(\lambda\frac{\partial T}{\partial x_i}\right), \tag{7}$$

where P is the pressure, τ_{ij} the stress tensor, and the heat flux is given by Fourier's law.

The rest of the system consists of the continuity equation

$$\frac{\partial \rho}{\partial t} + \frac{\partial}{\partial x_i}(\rho u_i) = 0, \tag{8}$$

the momentum equation

$$\frac{\partial}{\partial t}(\rho u_i) + \frac{\partial}{\partial x_j}(u_j \rho u_i) = -\frac{\partial P}{\partial x_i} + \frac{\partial \tau_{ij}}{\partial x_j},\tag{9}$$

and the equation of state

$$P = \rho R T.\tag{10}$$

In the present numerical simulations, the discontinuity is removed by replacing the Heaviside function by the smooth function

$$\mathcal{H}(G) \approx [1 + \tanh(G/\delta|\nabla G|)],\tag{11}$$

where δ is a small parameter of the order of the flame thickness.

The fully-compressible system (5)–(10) is solved using a high order compact scheme (Lele 1992) for spatial derivatives and a third order Runge-Kutta scheme (Wray 1990). Boundary conditions are treated following the method of Poinsot and Lele (1992). For one-dimensional calculations, the initial condition for the G function is

$$G(x) = \begin{cases} -1, & \text{if } x - x_f < -W; \\ \sin[\pi(x-x_f)/2W], & \text{if } |x - x_f| \le W; \\ 1, & \text{if } x - x_f > W, \end{cases}\tag{12}$$

and the boundary condition on G is treated in the same way as the other scalar variables. Here W is the thickness of the G profile. The converged one-dimensional solution is used as the initial condition for the two-dimensional calculation.

Figure 1 shows schematics of the two model problems considered, namely the flame response to (a) a steady harmonic velocity fluctuation, and (b) a pair of counter-rotating vortices. Some results for each model problem are presented and discussed below.

2.1.2 Harmonic inlet velocity

As shown in Fig. 1(a), we impose a steady harmonic inlet velocity profile

$$u(x = 0, t) = s_L^\circ + u' \cos(2\pi y).\tag{13}$$

For $u' = 0$, the G-field remains fixed at the initial condition. In a simulation, at $t = 0$ a finite value of u' is imposed at the inlet boundary; this velocity fluctuation then produces a curved front. The calculation proceeds until a final state is attained, in which the flame area does not change and the front moves toward the unburnt mixture due to the enhanced propagation rate. In the present calculation we used the parameter values $Re_a = (aL/\nu)_0 = 2000$, where a is the speed of sound, unity for the Prandtl and Lewis numbers, and $s_L^\circ/a = 0.05$. The results depend on the Markstein length $\mathcal{L}$ through the flame-speed variation (see (2)). To minimize this flame-structure effect and to extract the behavior of the flame in the Huygens' limit, we choose $\mathcal{L}/L = 0.01$ in the present calculation, where L is the width of the channel shown in Fig. 1(a).
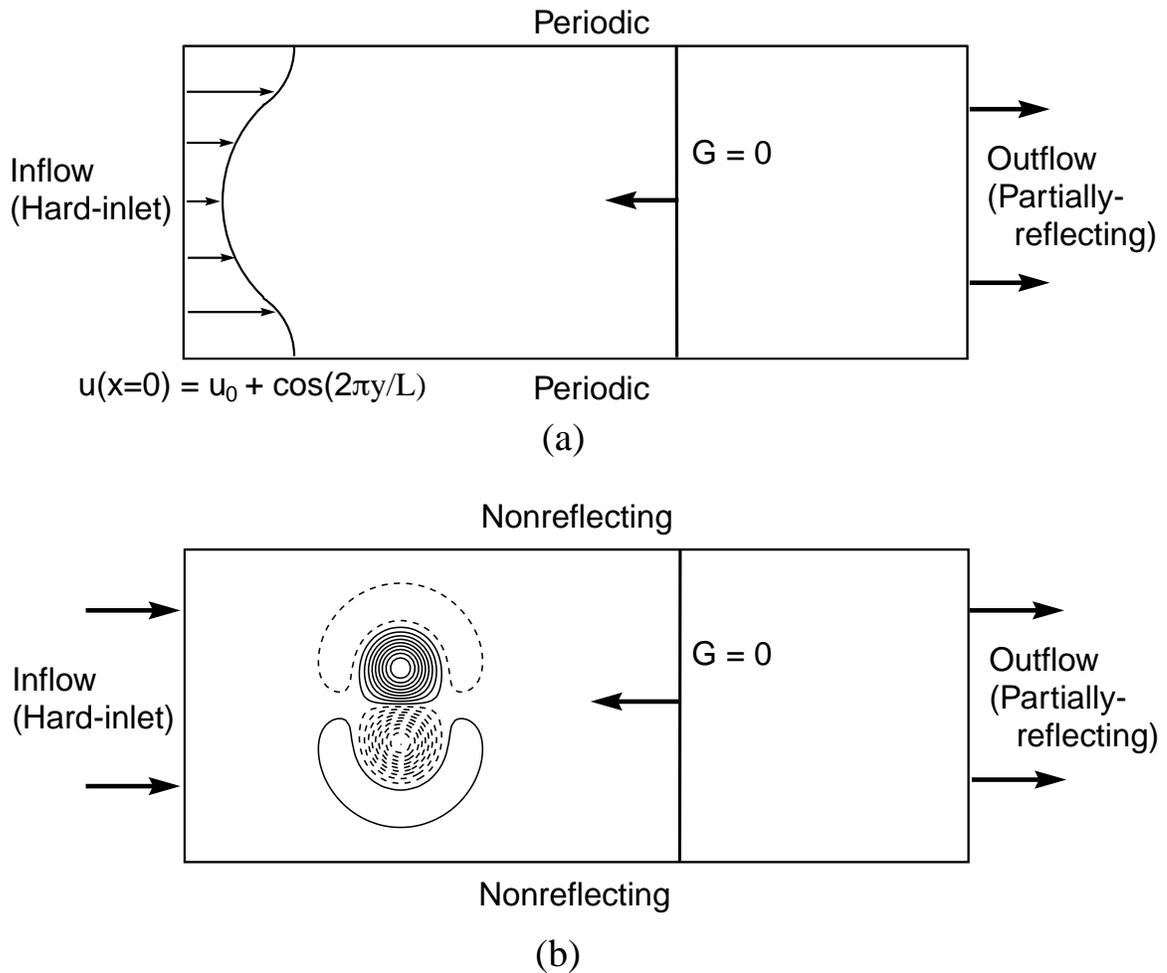
FIGURE 1. Schematics of the model problems and computational conditions: (a) flame propagating into the steady harmonic inlet velocity, (b) flame-vortex interaction, where the solid and dotted curves respectively denote positive and negative vorticities.

Figure 2 shows the final state of the flame fronts represented by the $G = 0$ contours for the inlet perturbations of $u'/s_L^\circ = 0$ and 0.3. Here $\alpha = (\rho_u - \rho_b)/\rho_u$ is the heat release parameter; $\alpha = 0$ for the zero heat-release case and $\alpha = 0.5$ when the downstream temperature is twice the upstream temperature. It is seen that the flames with heat release ($\alpha = 0.5$) are more curved than those without heat release ($\alpha = 0$). This is due to the hydrodynamic instability mechanism known as the Landau-Darrieus effect (Williams 1985). At a hydrodynamic discontinuity with constant propagation speed, thermal expansion induces a deflection of streamlines such that the convex front is further accelerated. Although the linear stability analysis predicts that the perturbation of the front grows indefinitely, in reality it saturates as nonlinear effects come into play. Figure 2 clearly demonstrates
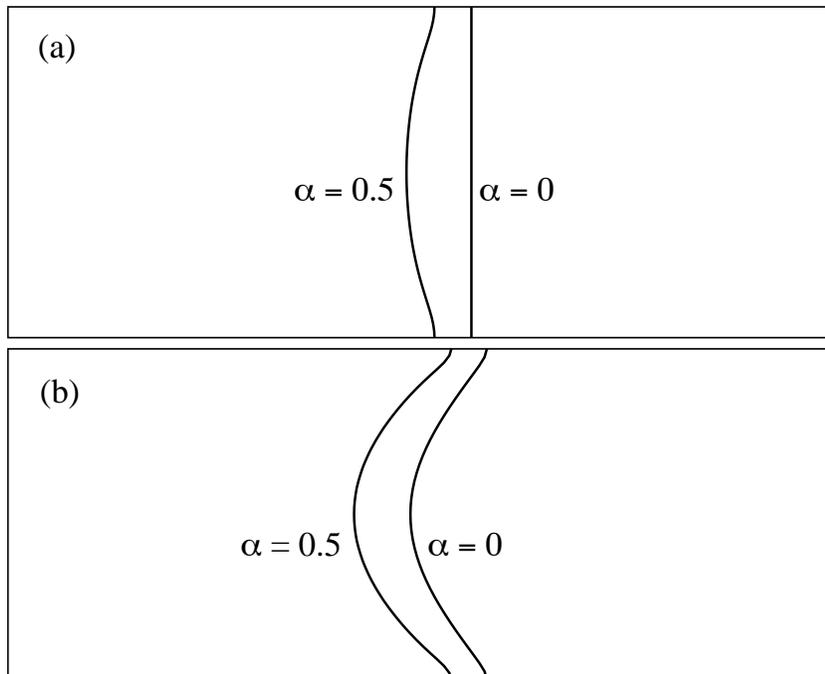
FIGURE 2. Flame fronts described as $G = 0$ contours subject to the steady harmonic inlet velocity for (a) $u'/s_L^\circ = 0$ and (b) $u'/s_L^\circ = 0.3$. Shown in each figure are the cases for zero heat release ($\alpha = 0$) and for $\alpha = 0.5$.

such behavior, and the flame propagating with larger heat release exhibits more wrinkling. In particular, it is of interest to note from Fig. 2(a) that with heat release the flame front does not remain planar even if inlet velocity perturbation is absent ($u' = 0$), consistent with the result of Cambray & Joulin (1992).

In Fig. 3 we plot the area ratio (A_T/A_L) as a function of the magnitude of velocity fluctuation (u'/s_L°) for the configuration shown in Fig. 1(a). At present, the range of u'/s_L° is limited due to numerical difficulty that arises when u' significantly exceeds s_L° so that the front forms sharp curvature. Nevertheless, Fig. 3 confirms the results of Cambray & Joulin (1992) in that there is an additional flame-speed enhancement due to thermal expansion for weak turbulence ($u'/s_L^\circ < 1$). For larger velocity fluctuations, it is expected that the effect of thermal expansion induced self-wrinkling of the front will be less prominent as the large convective flow field dominates the flame behavior, which may be a possible mechanism for the "bending" behavior. Further improvement in the numerical methodology to capture more excessive wrinkled front is required to obtain a more conclusive database regarding this issue.

2.1.3 Flame-vortex interaction

To further investigate the coupling between a flame and a flow via density variation, we adopt the flame-vortex interaction as a model problem, as was previously studied by Poinsot *et al.* (1991). In particular, the emphasis is on fundamental issues such as the flame front response to the vortical flows and attenuation and
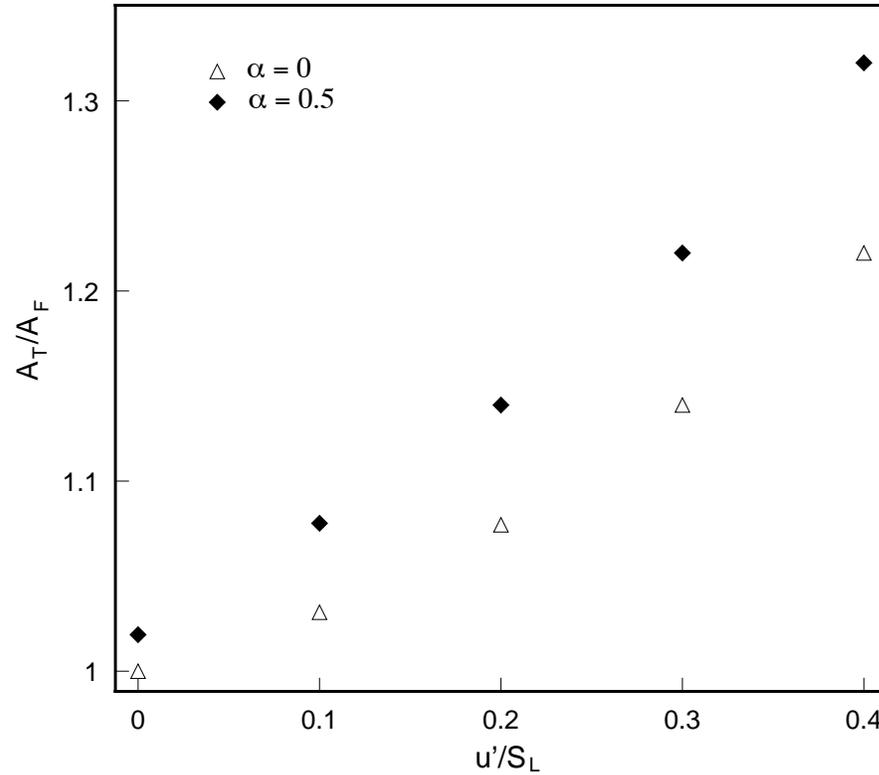
FIGURE 3. Nondimensional total flame-front area vs. nondimensional velocity fluctuation. Open symbols are for zero heat release ($\alpha = 0$) and solid symbols for $\alpha = 0.5$.

generation of vorticity by the flame due to thermal expansion. As shown in Fig. 1(b), at $t = 0$ we introduce a pair of counter-rotating vortices into the uniform flow field with $u_0 = s_L^\circ$, far upstream of the flame. Then, due to the mean flow as well as the flow induced by the vortices, the vortex pair drifts downstream and passes through the propagating flame front, while preserving symmetry. The initial circulation, Γ, of the vortices adopted in this study is given by

$$\Gamma(r) = \pm 2\pi \Psi \frac{r^2}{\sigma^2} \exp\left(-\frac{r^2}{\sigma^2}\right), \tag{14}$$

where r is the distance from the vortex center and σ the characteristic radius of the vortex. Here we define the strength of the vortex u' by the maximum circumferential velocity at $t = 0$. Other parameter values used in this study are $Re_a = 1000$, $Pr = Sc = 0.75$, $\mu/\mu_0 = (T/T_0)^{0.76}$, $s_L^\circ/a = 0.02$, $\mathcal{L}/(\lambda/\rho c_p s_L^\circ)_0 = 0.1$. The vortex diameter is initially about three times larger than the flame thickness and grows in time by diffusive transport.

Figures 4 and 5 show the snapshots of the flame front and vorticity contours at the instant that the flame is most wrinkled by the vortex, for two vortex strengths, $(u'/s_L^\circ)_{t=0} = 2.4$ and 4.8. In each figure, (a) is for the cold flame case ($\alpha = 0$)
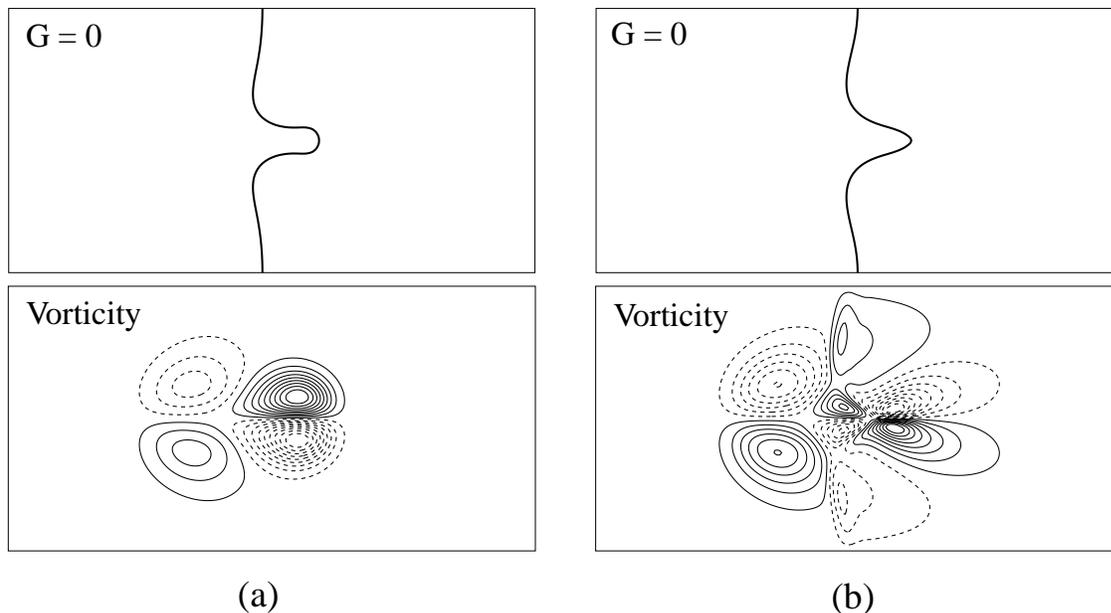
FIGURE 4. Flame-vortex interaction for $u'/s_L^\circ = 2.4$, (a) $\alpha = 0$ and (b) $\alpha = 0.75$. Top and bottom figures respectively denote flame fronts ($G = 0$) and vorticity. The solid and dotted curves respectively denote counterclockwise and clockwise vorticity.

and (b) for $\alpha = 0.75$. Although not presented here, the results of the G-equation model have been compared to that with the one-step Arrhenius chemistry, and it was found that the G-equation captures the essential physics of the flame and flow responses. It is also remarked that, due to the rapid decrease in the tangential velocity for the initial field (14), an additional vortex pair with opposite sign is formed behind the incident vortex pair. Although it may be unphysical, this fast-decaying vortex requires a smaller computational domain, and thus adopted in this qualitative study.

Figure 4 is for the lower vortex strength. It is seen that, while the vortices Fig. 4(a) preserve their original shapes through the flame, in Fig. 4(b) the vortices are significantly elongated behind the flame due to thermal expansion accelerating the flow. Furthermore, in this case it is interesting to note that the sign of the vorticity is reversed as the vortex passes through the flame. This demonstrates the vorticity generation due to the baroclinic torque mechanism arising from the fact that the pressure and density gradients are not parallel across the curved flame. In this configuration the flame-generated vorticity is opposite to the incident vorticity. Therefore, for the case shown in Fig. 4(b), the incident vortices is overridden by the flame-generated vortices and cannot survive the flame. Consequently, the reversed velocity field induced by the flame-generated vorticity tends to push the retarded flame front forward, yielding a less wrinkled front compared to the cold-flame case shown in Fig. 4(a). The results agrees qualitatively with a recent experimental observation (Mueller *et al.* 1995).

Figure 5 shows the case of a stronger vortex, $u'/s_L^\circ = 4.8$. The front becomes
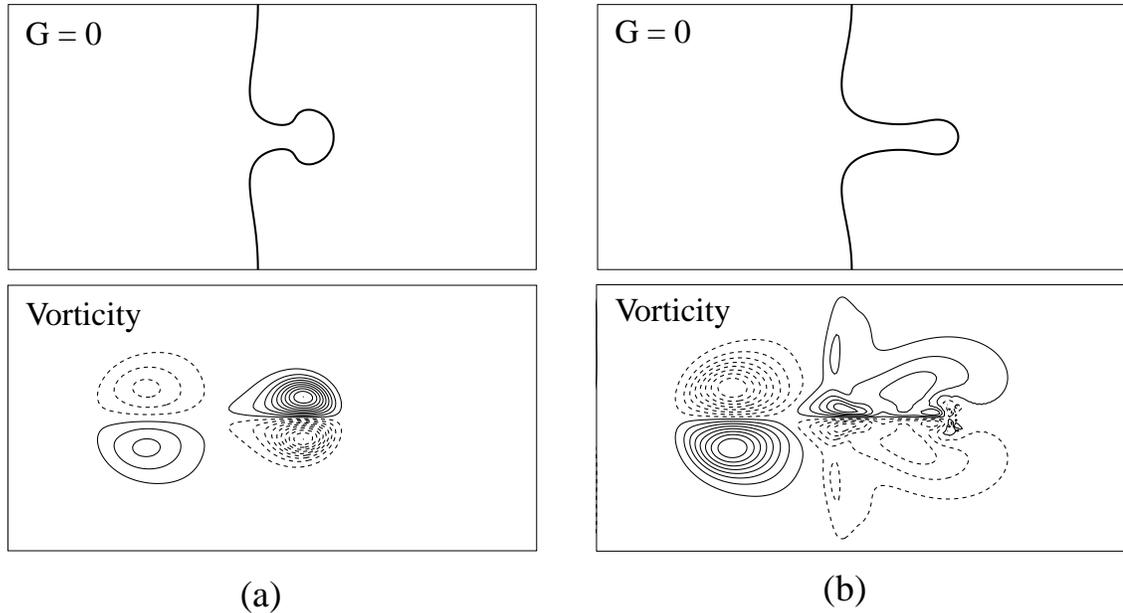
FIGURE 5. Flame-vortex interaction for $u'/s_L^\circ = 4.8$, (a) $\alpha = 0$ and (b) $\alpha = 0.75$. Top and bottom figures respectively denote flame fronts ($G = 0$) and vorticity. The solid and dotted curves respectively denote counterclockwise and clockwise vorticity.

more wrinkled. Consistent with the results in Fig. 4, it is seen that the flame-front wrinkling is less severe in the $\alpha = 0.75$ case. Unlike Fig. 4(b), however, the incident vortices shown in Fig. 5(b) are sufficiently strong to survive the flame, except around the sharply curved front where the flame-generated vorticity is most intense. Although the vorticity downstream of the flame has the same sign as the incident vorticity, the strength of the vorticity is considerably weakened. The mechanisms of the vorticity attenuation by the flame are the aforementioned flame-generated vorticity and volume expansion, which spreads out the vortical region while preserving the total circulation (cf. Mueller *et al.* 1995). These front-stabilizing effects may be partly responsible for the experimentally observed "bending" behavior of s_T at high turbulence levels, along with the hydrodynamic effect discussed in the previous subsection.

2.2 Dynamic subgrid-scale modeling for the G-equation

The main idea of the G-equation is to model flame structure as asymptotically thin front. This eliminates the highly nonlinear reaction terms and facilitates modeling for large-eddy simulation. In high Reynolds-number flows, a turbulent premixed flame can be viewed as a wrinkled flame "brush" propagating with velocity s_T. Several previous studies have attempted to derive explicit expressions for $s_T(u')$ (Clavin & Williams 1979, Yakhot 1988a, Kerstein and Ashurst 1992). If u' represents the grid-size averaged quantity, this approach is analogous to the original Smagorinsky's subgrid scale model for Navier-Stokes equation in which the eddy viscosity coefficient is given *a priori*. Unfortunately, the existing theoretical and empirical results for $s_T(u')$ do not agree with one another, so that finding the correct functional form

of $s_T(u')$ remains an open question. Even if the question is resolved, there will still be a constant to be determined.

In this section we suggest a new subgrid-scale model for the G-equation based on the dynamic modeling principle developed recently (Germano *et al.* 1991, Moin *et al.* 1991). One of the prerequisite conditions for the application of dynamic subgrid-scale modeling is that the equation be scale-invariant so that the subgrid quantities can be extrapolated from two adjacent scales. The scale-invariance of the G-equation has been discussed in the previous studies (Pocheau 1992, Yakhot 1988b), and was employed in renormalization group theory to derive an explicit formula for $s_T(u')$ (Yakhot 1988a). We shall skip detailed discussion of this issue.

We start from the simplest incompressible form of the G-equation;

$$\frac{\partial G}{\partial t} + \frac{\partial}{\partial x_j}\left(u_j G\right) = s_L |\nabla G|, \tag{15}$$

where, although not essential, s_L is assumed to be constant. Following previous works, we define the "grid" filter $\bar{\mathcal{G}}$ and the "test" filter $\hat{\mathcal{G}}$ respectively as

$$\bar{f}(\mathbf{x}) = \int f(\mathbf{x}')\bar{\mathcal{G}}(\mathbf{x}, \mathbf{x}')d\mathbf{x}', \quad \hat{f}(\mathbf{x}) = \int f(\mathbf{x}')\hat{\mathcal{G}}(\mathbf{x}, \mathbf{x}')d\mathbf{x}', \tag{16}$$

where the width of the test filter, $\hat{\bar{\Delta}}$, is larger than that of the grid filter, $\bar{\Delta}$. By applying the grid filter to (16), we obtain

$$\frac{\partial \bar{G}}{\partial t} + \frac{\partial}{\partial x_j}\left(\bar{u}_j \bar{G}\right) = -\frac{\partial}{\partial x_j}\left(\overline{u_j G} - \bar{u}\bar{G}\right) + s_L \overline{|\nabla G|}. \tag{17}$$

Here both the subgrid scalar flux $\overline{u_j G} - \bar{u}_j \bar{G}$ and the filtered modulus term $\overline{|\nabla G|}$ need to be modeled. We proceed with applying the test filter, then (17) becomes

$$\frac{\partial \hat{\bar{G}}}{\partial t} + \frac{\partial}{\partial x_j}\left(\hat{\bar{u}}_j \hat{\bar{G}}\right) = -\frac{\partial}{\partial x_j}\left(\widehat{\overline{u_j G}} - \hat{\bar{u}}_j \hat{\bar{G}}\right) + s_L \widehat{\overline{|\nabla G|}}. \tag{18}$$

In (17) and (18), it is the filtered modulus term, $\overline{|\nabla G|}$ that makes the subgrid scale modeling of the G-equation difficult compared to other scalar equations. The simplest solution is to eliminate this term by applying the test filter to (17) and subtract from (18), yielding

$$(18) - \widehat{(17)} = -\frac{\partial}{\partial x_j}\left(\widehat{\bar{u}_j \bar{G}} - \hat{\bar{u}}_j \hat{\bar{G}}\right), \tag{19}$$

where all the quantities on RHS can now be calculated directly from the large-eddy grid solutions.

We now need to introduce a model to represent the subgrid-scale quantities of the G-equation. To this end, we adopt the viewpoint described at the beginning of

the subsection, *i.e.* that, on the large-eddy scale, the turbulent flame brush can be represented as a thick front which propagates at speed s_T. Equations (17) and (18) can then be written as

$$\frac{\partial \bar{G}}{\partial t} + \frac{\partial}{\partial x_j}\left(\bar{u}_j \bar{G}\right) = \bar{s}_T |\nabla \bar{G}|, \tag{20}$$

$$\frac{\partial \hat{\bar{G}}}{\partial t} + \frac{\partial}{\partial x_j}\left(\hat{\bar{u}}_j \hat{\bar{G}}\right) = \hat{\bar{s}}_T |\nabla \hat{\bar{G}}|, \tag{21}$$

where $\bar{s}_T$ and $\hat{\bar{s}}_T$ respectively represent the speed of the flame brush at $\bar{\Delta}$ and $\hat{\bar{\Delta}}$ scales. To relate s_T with the turbulence intensity u', we choose a linear form

$$\bar{s}_T/s_L \approx 1 + C(u'/s_L). \tag{22}$$

Even if the linear form is not correct, the error may be adjusted by the constant C through the dynamic procedure.

As in the eddy-viscosity model, we further assume $u' \sim \bar{\Delta}|\bar{S}|$, where $|\bar{S}| = |2\bar{S}_{ij}\bar{S}_{ij}|^{1/2}$ of the large scale strain rate tensor

$$\bar{S}_{ij} = \frac{1}{2}\left(\frac{\partial \bar{u}_i}{\partial x_j} + \frac{\partial \bar{u}_j}{\partial x_i}\right). \tag{23}$$

Therefore, $\bar{s}_T$ and $\hat{\bar{s}}_T$ can be modeled as

$$\frac{\bar{s}_T}{s_L} = 1 + C_G\left(\frac{\bar{\Delta}|\bar{S}|}{s_L}\right), \tag{24}$$

$$\frac{\hat{\bar{s}}_T}{s_L} = 1 + C_G\left(\frac{\hat{\bar{\Delta}}|\hat{\bar{S}}|}{s_L}\right). \tag{25}$$

Substituting (24) and (25) into (20) and (21) and combining with (19) we obtain

$$\left\{1 + C_G\left(\frac{\hat{\bar{\Delta}}|\hat{\bar{S}}|}{s_L}\right)\right\}|\nabla \hat{\bar{G}}| - \widehat{\left\{1 + C_G\left(\frac{\bar{\Delta}|\bar{S}|}{s_L}\right)\right\}|\nabla \bar{G}|} = -\frac{1}{s_L}\frac{\partial}{\partial x_j}\left(\widehat{\bar{u}_j \bar{G}} - \hat{\bar{u}}_j \hat{\bar{G}}\right), \tag{26}$$

which we wish to use to determine the constant C_G. This is a version of Germano's identity (Germano *et al.* 1991) for the G-equation. Unlike Germano's identity used in the Navier-Stokes and other scalar equations, however, here we subtract the entire equations (17) and (18) instead of treating the subgrid stress terms only, in order to eliminate the modulus term $\widehat{|\nabla G|}$ which is difficult to model. Consequently, the resulting identity (26) is a single scalar equation for a single unknown parameter C_G, rather than the three equations arising from the models for other scalar equations.

As in previous work on dynamic subgrid-scale models, the constant C_G is, in general, a function of space and time. Therefore, C_G cannot be taken out of the test filter, and (26) is an integral equation. However, if the problem of interest has at least one homogeneous direction, then C_G can be assumed to be a function of the other coordinates and can be removed from the test filter. For example, in the case of premixed flame propagating through a channel that is homogeneous in y- and z-directions, $C_G = C_G(x, t)$ so that

$$
C_G(x_0, t) \left\{ \left(\frac{\hat{\bar{\Delta}}|\hat{\bar{S}}|}{s_L} \right) |\nabla \hat{\bar{G}}| - \widehat{\left(\frac{\bar{\Delta}|\bar{S}|}{s_L} \right) |\nabla \bar{G}|} \right\} = \widehat{|\nabla \bar{G}|} - |\nabla \hat{\bar{G}}| - \frac{1}{s_L} \frac{\partial}{\partial x_j} \left(\widehat{\bar{u}_j \bar{G}} - \hat{\bar{u}}_j \hat{\bar{G}} \right),
$$

$$(27)$$

which is a simpler algebraic equation.

The modeling proposed in this study is for the simplest constant-density case. However, it is anticipated that the same principle can be extended to incorporate variable density consideration. The validity of the model is currently under investigation for the incompressible G-equation model in homogeneous turbulence.

3. Future work

In this study the G-equation model has been applied to several fundamental problems relevant to turbulent premixed combustion in the laminar flamelet regime. Furthermore, a preliminary dynamic subgrid-scale model for the G-equation has been proposed. These ideas need to be further improved to be applied to practical high-Reynolds number premixed combustion systems.

From the standpoint of computational efficiency, the numerical techniques used in the present study appear to have a limited application in the practical turbulent reacting flows, partly due to necessity of resolving the abrupt changes in the dependent variables across the flame front. It is anticipated that a more efficient discontinuity-capturing numerical scheme will greatly reduce the computational cost, thereby allowing more extensive parametric studies of fundamental issues such as turbulent flame speed.

As the next step in the application of the large-eddy simulation to combustion, the dynamic subgrid-scale model for the G-equation suggested in this study should be validated by the direct numerical simulation of the passive G-equation in a turbulent flow. If it proves to be successful, then further study is needed to extend the model to account for the effects of thermal expansion and variable flame speed.

REFERENCES

BRADLEY, D. 1992 How fast can we burn? *Twenty-Fourth Symposium (International) on Combustion*, The Combustion Institute, pp. 247-262.

CAMBRAY, P. & JOULIN, G. 1992 On moderately-forced premixed flames. *Twenty-Fourth Symposium (International) on Combustion,* The Combustion Institute, pp. 61-67.

CLAVIN, P. & WILLIAMS, F. A. 1979 Theory of premixed-flame propagation in large-scale turbulence. *J. Fluid Mech.* **90,** 589.

DAMKÖHLER, G. 1940 *Z. Elektrochem.* **46,** 601.

GERMANO, M., PIOMELLI, U., MOIN, P. & CABOT, W. H. 1991 A dynamic subgrid-scale eddy viscosity model. *Phys. Fluids A.* **3,** 1760.

KERSTEIN, A. R. & ASHURST, WM. T. 1992 Propagation rate of growing interfaces in stirred fluids. *Phys. Rev. Lett.* **68,** 934.

KERSTEIN, A. R. & ASHURST, WM. T. 1994 Passage rates of propagating interfaces in randomly advected media and heterogeneous media. *Phys. Rev. E.* **50,** 1100.

KERSTEIN, A. R., ASHURST, WM. T., & WILLIAMS, F. A. 1988 Field equation for interface propagation in an unsteady homogeneous flow field. *Phys. Rev. A.* **37,** 2728.

LELE, S. 1992 Compact finite difference schemes with spectral-like resolution. *J. Comp. Phys.* **103,** 16.

LIÑÁN, A. & WILLIAMS, F. A. 1993 *Fundamental aspects of combustion,* Oxford University Press.

MICHELSON, D. M. & SIVASHINSKY, G. I. 1977 Non-linear analysis of hydrodynamic instability in laminar flames; Part II: numerical experiments. *Acta Astronautica.* **4,** 1207.

MOIN, P., SQUIRES, K., CABOT, W. & LEE, S. 1991 A dynamic subgrid-scale model for compressible turbulence and scalar transport. *Phys. Fluids A.* **3,** 2746.

MUELLER, C. J., DRISCOLL, J. F., REUSS, D. L., DRAKE, M. C. & ROSALIK, M. E. 1995 Generation and attenuation of vorticity by flames: Measured vorticity field time evolution during a premixed flame-vortex interaction. *Fall Technical Meeting of the Western States Section of the Combustion Institute,* Paper 95F-217, Stanford University, Stanford, CA, Oct. 30-31.

PELCE, P. AND CLAVIN, P. 1982 Influence of hydrodynamics and diffusion upon the stability limits of laminar premixed flames. *J. Fluid Mech.* **124,** 219.

PETERS, N. 1992 A spectral closure for premixed turbulent combustion in the flamelet regime. *J. Fluid Mech.* **242,** 611.

POINSOT, T. & LELE, S. 1992 Boundary conditions for direct simulations of compressible viscous flows. *J. Comp. Phys.* **101,** 104.

POCHEAU, A. 1992 Front propagation in a turbulent medium. *Europhysics Letters.* **20**, 401.

WILLIAMS, F. A. 1985 *Combustion Theory*, 2nd ed., Addison-Wesley.

WRAY, A. A. 1990 Minimal storage time-advancement schemes for spectral methods. *Internal Report,* NASA Ames.

YAKHOT, V. 1988a Propagation velocity of premixed turbulent flames. *Comb. Sci. & Tech.* **60**, 191.

YAKHOT, V. 1988b Scale invariant solutions of the theory of thin turbulent flame propagation. *Comb. Sci. & Tech.* **62**, 127.